Difference in magnetic and ferroelectric properties between rhombohedral and hexagonal polytypes of AgFeO_{2}: A single-crystal study

Noriki Terada, Yuta Ikedo, Hirohiko Sato, Dmitry D. Khalyavin, Pascal Manuel, Fabio Orlandi, Yoshihiro Tsujimoto, Yoshitaka Matsushita, Atsushi Miyake, Akira Matsuo, Masashi Tokunaga, and Koichi Kindo

Phys. Rev. B **99**, 064402 — Published 1 February 2019

DOI: 10.1103/PhysRevB.99.064402

Difference in magnetic and ferroelectric properties between rhombohedral and hexagonal polytypes of $AgFeO_2$: a single crystal study

Noriki Terada[1],* Yuta Ikedo[2], Hirohiko Sato[2],† Dmitry D. Khalyavin[3], Pascal Manuel[3], Fabio Orlandi[3], Yoshihiro Tsujimoto[1], Yoshitaka Matsushita[1], Atsushi Miyake[4], Akira Matsuo[4], Masashi Tokunaga[4], and Koichi Kindo[4]

[1]*National Institute for Materials Science, Sengen 1-2-1, Tsukuba, Ibaraki 305-0047, Japan*

[2]*Department of Physics, Chuo University, 1-13-27 Kasuga, Bunkyo-ku, Tokyo 112-8551, Japan*

[3]*ISIS facility, STFC Rutherford Appleton Laboratory, Chilton, Didcot, Oxfordshire, OX11 0QX, United Kingdom and*

[4]*Institute for Solid State Physics, University of Tokyo, 5-1-5 Kashiwanoha, Kashiwa, Chiba 277-8581, Japan*

(Dated: January 14, 2019)

We have investigated magnetic and dielectric properties of rhombohedral 3R-$AgFeO_2$ and hexagonal 2H-$AgFeO_2$, by using magnetic and dielectric bulk measurements and neutron diffraction experiment with single crystals grown by a hydrothermal synthesis. Magnetic phase transitions occur at T =14.0 K and T =6.0 K in 3R-$AgFeO_2$, and T =17.0 K and T =9.5 K in 2H-$AgFeO_2$ under zero magnetic field. Multistep metamagnetic phase transitions were observed in 3R-$AgFeO_2$ in magnetization measurements up to 60 T, while a single phase transition occurs in 2H-$AgFeO_2$. The ferroelectric polarization parallel and perpendicular to the triangular lattice plane appears below T = 6.0 K in 3R-$AgFeO_2$, which is concomitant with onset of the cycloid magnetic ordering with the propagation vector $\boldsymbol{k} = (-\frac{1}{2}, q, \frac{1}{2}; q \simeq 0.2)$ and the magnetic point group polar $m1'$. On the other hand, the ferroelectric polarization is absent even below the lower phase transition temperature in 2H-$AgFeO_2$, which can be explained by the proper screw magnetic structure with $\boldsymbol{k} = (0, q, 0; q \simeq 0.4)$ and the nonpolar $2221'$ point group. Although the two dimensional triangular lattice layers of Fe^{3+} are common in the two polytypes, the magnetic and ferroelectric properties are significantly different. The emergence of ferroelectric polarization which is not confined to be within the plane of cycloid for 3R-$AgFeO_2$ can be explained by the extended inverse Dzyloshinskii-Moriya effect with two orthogonal components, $\boldsymbol{p}_1 \propto \boldsymbol{r}_{ij} \times [\boldsymbol{S}_i \times \boldsymbol{S}_j]$ and $\boldsymbol{p}_2 \propto \boldsymbol{S}_i \times \boldsymbol{S}_j$. Unlike other delafossite compounds, the $\boldsymbol{p}_2$ component is not allowed in the proper screw phase of 2H-$AgFeO_2$ due to the symmetry restriction of the parent space group.

PACS numbers: 75.80.+q, 75.50.Ee, 75.25.+z, 77.80.-e

I. INTRODUCTION

Magnetoelectric multiferroic compounds, which possess ferroelectric and (anti)ferromagnetic orderings, have attracted much attention in last fifteen years.[1–3] Delafossite family compounds ABO_2 (A = Cu, Ag, B =Cr, Fe) with the $R\bar{3}m$ space group have given great opportunities to study coupling mechanism between magnetic and ferroelectric orderings in multiferroics.[4] In the delafossites, there are various types of magnetic orderings including noncollinear structures coupled to ferroelectricity. The coupling mechanisms for noncollinear spin structures, which are called the inverse Dzyaloshinskii-Moriya (DM) effect[5,6] and the spin current mechanism[7], have been proposed by the theoretical papers, showing that the electric dipole moments, $\boldsymbol{p}$, generated by a pair of neighboring spins, $\boldsymbol{S}_i$ and $\boldsymbol{S}_j$, are expressed as $\boldsymbol{p} \propto \boldsymbol{r}_{ij} \times [\boldsymbol{S}_i \times \boldsymbol{S}_j] (\equiv \boldsymbol{p}_1)$. In the specific cases, such as the orthorhombic perovskite with $Pbnm$ space group and a cycloid structure $\boldsymbol{r}_{ij} \perp [\boldsymbol{S}_i \times \boldsymbol{S}_j]$, the theory can well explain the ferroelectric polarization.[8,9]

In $CuFeO_2$ and $CuCrO_2$, however, the proper screw magnetic ordering also induces the ferroelectric polarization parallel to the vector product of neighboring spins, $\boldsymbol{p} || [\boldsymbol{S}_i \times \boldsymbol{S}_j]$, in spite of $\boldsymbol{p}_1 = 0$ due to $\boldsymbol{r}_{ij} || [\boldsymbol{S}_i \times \boldsymbol{S}_j]$.[10–18] Kaplan and Mahanti have extended the inverse DM mechanism to general symmetry conditions,[19] which can explain the polarization parallel to $\boldsymbol{S}_i \times \boldsymbol{S}_j$ in the proper screw ordering, which is orthogonal to the $\boldsymbol{p}_1$ componens, $\boldsymbol{p} \propto \boldsymbol{S}_i \times \boldsymbol{S}_j$ ($\equiv \boldsymbol{p}_2$). In some other multiferroics with the proper screw ordering, the ferroelectric polarization parallel to $\boldsymbol{S}_i \times \boldsymbol{S}_j$ has been reported.[20–22] The mechanism is applicable for the cycloid magnetic structure ($\boldsymbol{r}_{ij} \perp [\boldsymbol{S}_i \times \boldsymbol{S}_j]$) as well as the proper screw case. For example, the ferroelectric polarization parallel to $\boldsymbol{S}_i \times \boldsymbol{S}_j$ in additional to the dominant polarization along the trigonal axis has been reported in the cycloidal phase in $BiFeO_3$.[23]

The magnetic and dielectric properties of the silver delafossite ferrite, 3R-$AgFeO_2$ ($R\bar{3}m$), have been investigated in previous work using powder sample.[24] There are two magnetic phase transitions at T =15 K and 9 K in 3R-$AgFeO_2$. A collinear spin-density-wave (SDW) ordering is stabilized for 9 K $\leq T \leq$ 15 K, while it turns into the cycloid ordering with spin components confined to the hexagonal [110]-[001] plane below T = 9 K. Although a ferroelectric polarization appears below the lower phase transition and the polarization direction was predicted to be sum of the two orthogonal components, $\boldsymbol{p}_1$ and $\boldsymbol{p}_2$,[24] the direction of polarization was experimentally unclear due to the only 3R-$AgFeO_2$ powder sample available at that time.

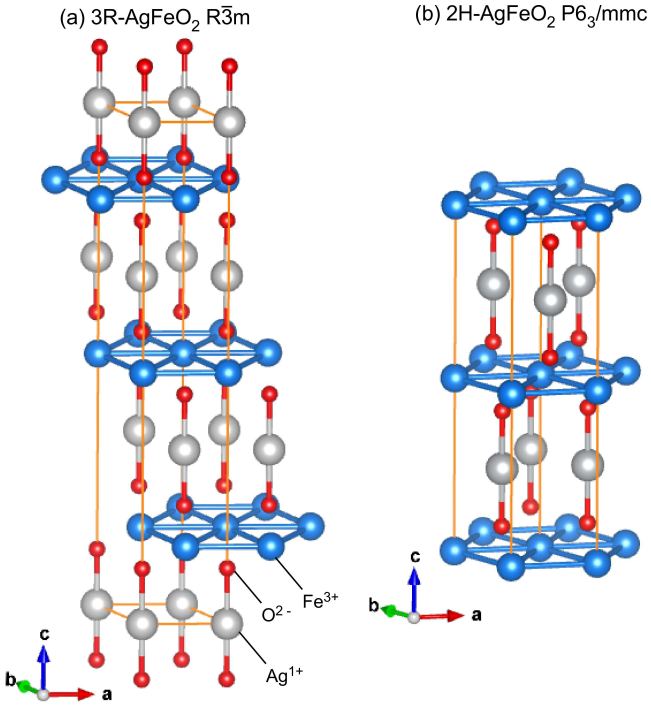

FIG. 1: (color online) Crystal structures of (a)3R-$AgFeO_2$ ($R\bar{3}m$) and (b)2H-$AgFeO_2$ ($P6_3/mmc$). The lattice parameters for 3R-$AgFeO_2$ are a = 3.0391 Å, c = 18.590 Å; Ag(0,0,0), Fe(0,0,0.5), O(0,0,0.1112)),[26] and those for 2H-$AgFeO_2$ are a = 3.039 Å, c = 12.395 Å; Ag(1/3,2/3,0.25), Fe(0,0,0), O(1/3,2/3,0.0833).[27]

There is the other polytype with the hexagonal space group $P6_3/mmc$, 2H-$AgFeO_2$, with very similar crystal structure to 3R-$AgFeO_2$. As illustrated in Fig. 1, whereas the two dimensional triangular lattice layers of Fe^{3+} are common in the two polytypes, the stacking sequences are different, ABCABC... in 3R-$AgFeO_2$ or $AA'AA'$... in 2H-$AgFeO_2$. The previous powder study for 2H-$AgFeO_2$ argued that the difference in the parent space group, rhombohedral or hexagonal, affects the ferroelectric polarization at low temperature in of $AgFeO_2$ significantly.[28] In 2H-$AgFeO_2$, there exist several magnetic phases which are a SDW (11 K $\leq T \leq$ 18 K), a proper screw ($T \leq$ 14 K), and a general spiral phases below T = 5.5 K, which are coexistent with each other even at the lowest temperature. The emergence of ferroelectric polarization is concomitant with onset of the general spiral order. The proper screw ordering does not generate the polarization in the hexagonal polytype 2H-$AgFeO_2$, which is significantly different from the case in 3R-CuBO_2 (B = Cr and Fe). However, the previous work could not determine the true ground state owing to the phase coexistence of the powder sample in 2H-$AgFeO_2$.[28]

Recently, we have succeeded in growing single crystals of both 3R-$AgFeO_2$ and 2H-$AgFeO_2$ by using the hydrothermal synthesis method. In the present study, we extend the powder studies,[24,28] and clearly investigate the magnetic phase transitions and the difference in the ferroelectric polarization induced by the noncollinear orderings by using the single crystals of the two polytypes of $AgFeO_2$. We performed magnetization, dielectric permittivity, pyroelectric current measurements and the neutron diffraction experiments on single crystal samples of 3R-$AgFeO_2$ and 2H-$AgFeO_2$.

II. EXPERIMENTAL DETAILS

Single crystals of 3R-$AgFeO_2$ and 2H-$AgFeO_2$ were grown using a hydrothermal method. In this process, the starting materials, Fe_2O_3 and Ag_2O, were sealed in a silver capsule with a small amount of RbOH. This mixture was kept at 650 °C and 150 MPa for two days. After the reaction, hexagonal plates of both 3R-$AgFeO_2$ and 2H-$AgFeO_2$ with a typical thickness of 0.5 mm, as shown in Figs. 2(a) and 2(b), were obtained. It infers that these polytypes can be grown under very similar conditions. By single crystal X-ray diffraction experiments, carried out at T = 113 K for 3R-$AgFeO_2$ and T = 293 K for 2H-$AgFeO_2$, we confirmed that these were single crystals.[29] The two polytypes can be distinguished by seeing the difference in the diffraction patterns,[30] for example $L = 3n$ (n is ingeger) in 3R-$AgFeO_2$ and $L = 2n$ in $AgFeO_2$ along the c^*-direction. X-ray Laue images are shown in Figs. 2(a) and 2(b). We confirmed that there is no magnetic impurity with ferromagnetic component, such as Fe_2O_3 by magnetization measurements on the single crystal.

Magnetization up to 6.0 T was measured using a magnetic property measurement system (Quantum Design, MPMS-XL). Magnetization at higher magnetic fields up to 60 T was measured using a pulsed magnet at the Institute for Solid State Physics (ISSP) in the University of Tokyo. Dielectric permittivity and pyroelectric current measurements were performed with a physical properties measurement system (Quantum Design, PPMS). The dielectric permittivity and pyroelectric current were determined using an LCR meter (Agilent, E4980A) and an electrometer (Keithley, 6517B), respectively. Frequencies of 100 kHz and 1 MHz were employed for the dielectric permittivity measurements. During pyroelectric current measurements, the sample was first cooled under a poling electric field up to ±800 kV/m, and subsequenly the pyroelectric current was recorded on warming in zero electric field. Integrating the current with respect to time gave the dielectric polarization. We confirmed that the sign of the dielectric polarization was reversed when reversing the poling electric field. For pyroelectric current measurement under a pulsed magnetic field up to 40 T in ISSP, after cooling under pooling electric field, we measured the current without electric field during sweeping a magnetic field. We applied magnetic fields along one of three equivalent [110] directions in the case of B_{ab} and along the hexagonal c-axis in the case of B_c.

Single crystal neutron diffraction measurements were

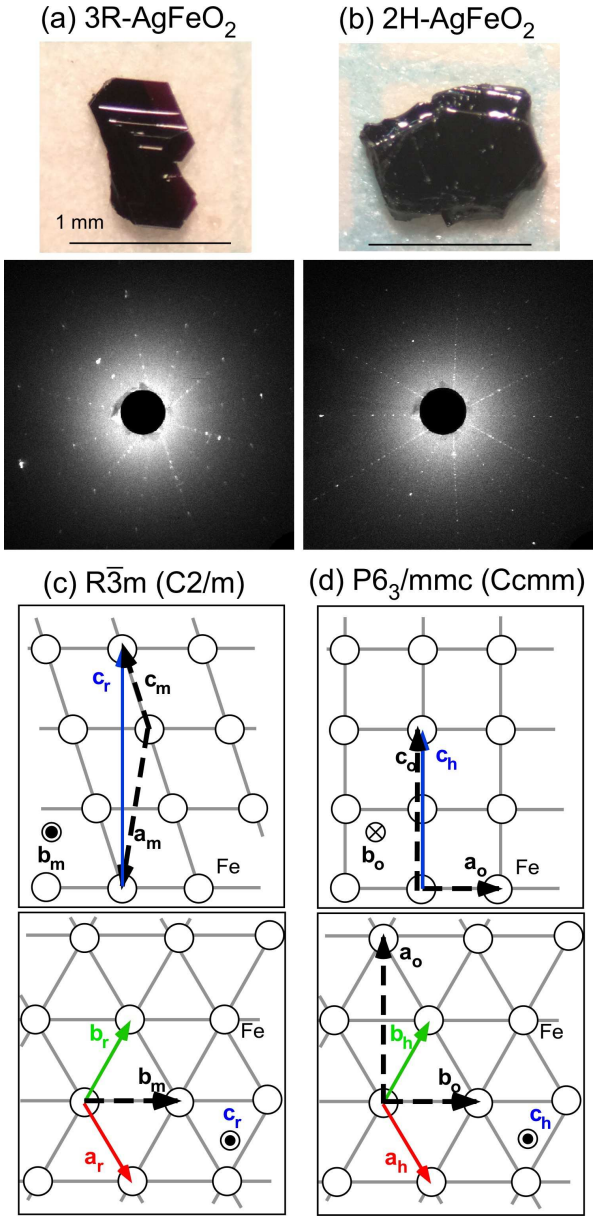

FIG. 2: (color online) Photographs and X-ray Laue images of the hexagonal c direction of the single crystals of (a)3R-$AgFeO_2$ and (b)2H-$AgFeO_2$. Relationship of the unit cell basis vectors between above and below the magnetic phase transition temperatures: (c)$R\bar{3}m$ and $C2/m$ in 3R-$AgFeO_2$ and (d)$P6_3/mmc$ and $Ccmm$ in 2H-$AgFeO_2$ space groups. The subscripts, r, m, h, and o, denote unit vectors for $R\bar{3}m$ (hexagonal setting), $C2/m$, $P6_3/mmc$, and $Ccmm$, respectively.

carried out using the WISH cold neutron time-of-flight diffractometer[31] at the ISIS Facility of the Rutherford Appleton Laboratory (UK). The single crystal was mounted on a standard He cryostat with the hexagonal $[1\bar{1}0]$-axis vertical. Since the WISH diffractometer has a pair of widely coverage area detectors with ±15 degrees in vertical direction, we can provide access to out of scattering plane of the hexagonal (H, H, L) (monoclinic $(2\bar{H}, K, H)$ in 3R-$AgFeO_2$ and orthorhombic $(0, K, L)$ planes in 2H-$AgFeO_2$). We use monoclinic notation in 3R-$AgFeO_2$ and orthorhombic notation in 2H-$AgFeO_2$ unless otherwise specified. Because, since magnetic orderings lower the symmetries down to monoclinic in 3R-$AgFeO_2$ and orthorhombic in 2H-$AgFeO_2$ below magnetic phase transition temperatures, it is convenient to use these low symmetry notations. Actually, in previous powder neutron diffraction experiments,[24,25,28], nuclear peak splittings and broadenings indicating losing the three fold and six fold rotational symmetry elements of $R\bar{3}m$ and $P6_3/mmc$ in 3R-$AgFeO_2$ and 2H-$AgFeO_2$, respectively. The results imply symmetry lowering down to at least the maximal non-isomorphic subgroup $C2/m$ in 3R-$AgFeO_2$ and $Ccmm$ in 2H-$AgFeO_2$, which takes into account only the coupling of the magnetic order parameter to the macroscopic strains. The relationships between the rhombohedral (hexagonal setting) and monoclinic bases, and the hexagonal and orthorhombic bases are illustrated in Figs. 2(c) and 2(d). Crystal and magnetic structure refinements were performed using the FullProf program.[32]

III. EXPERIMENTAL RESULTS

A. Magnetization

3R-$AgFeO_2$– Temperature dependences of magnetic susceptibility ($\chi(T)$) under a magnetic field perpendicular to the hexagonal c axis (B_{ab}) and parallel to the c axis (B_c) up to 6 T for 3R-$AgFeO_2$ are shown in Figs. 3(a) and 3(b). A small peak anomaly was observed at $T = 14$ K in both the directions, while $\chi(T)$ exhibits a sharp drop at $T = 5.5$ K in B_{ab}= 0.1 T and $B_c = 0.1$ T. As reported in the previous powder study,[24] these anomalies are expected to be the magnetic phase transitions from the paramagnetic phase to incommensurate phase (ICM1), and from ICM1 to ICM2 phases. The phase transition temperatures, $T = 14$ K and 5.5 K, of the single crystal, are not perfectly consistent with those of the powder sample ($T = 15$ K and 9 K).[24] Although the inconsistency between powder and single crystal samples has not been fully understood, the difference in the sample quality might affect the stability of magnetic ordering in 3R-$AgFeO_2$, as similarly seen in other frustrated systems.[33–35] The higher transition temperature is independent of the magnetic fields. While the lower transition temperature is not affected by B_{ab}, it gradually decreases with increasing B_c as illustrated by the dotted lines in Figs. 3(a) and 3(b).

We measured the magnetization processes at $T = 1.3$ K in B_{ab} and B_c in 3R-$AgFeO_2$, which are shown in Figs. 4(a) and 4(b). The magnetization exhibits no clear anomaly in B_{ab} up to 60 T apart from a slight change in the slope around 40 T shown in Fig. 4(a).

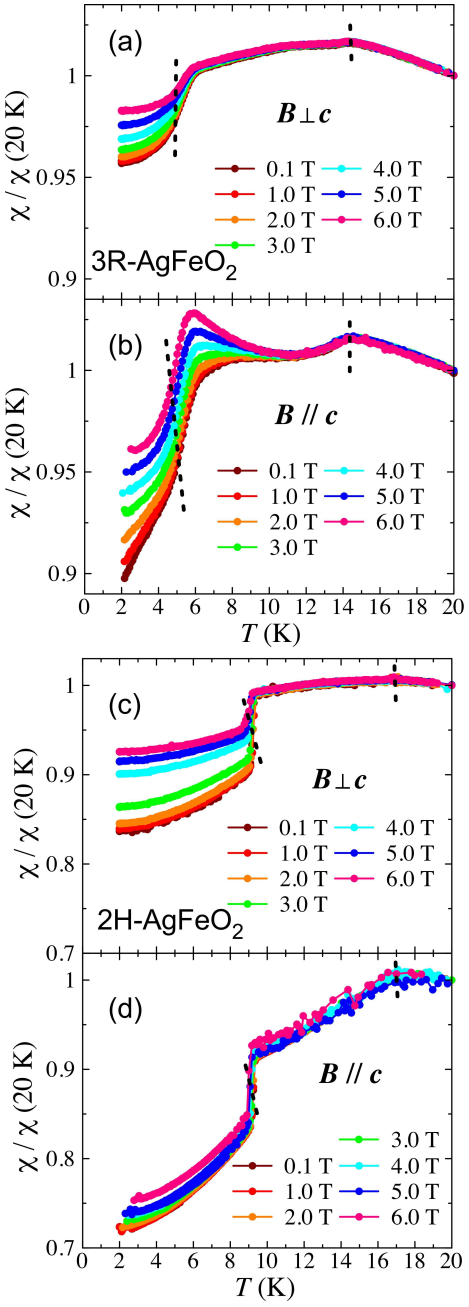

FIG. 3: (color online) Temperature dependence of magnetic susceptibility under magnetic fields perpendicular to (a) hexagonal c axis and (b) parallel to the c axis in 3R-$AgFeO_2$. (c) and (d) are the data for 2H-$AgFeO_2$. These data were normalized to the value at $T = 20$ K. The dotted lines show the magnetic phase transition temperatures.

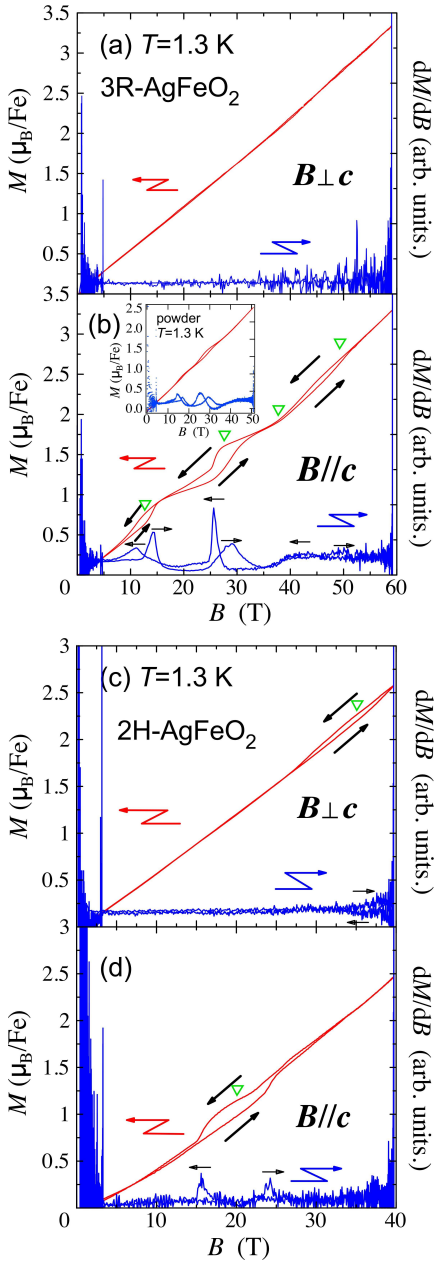

FIG. 4: (color online) Magnetization processes and the derivative of magnetization with respect to the magnetic field (dM/dB) under pulsed magnetic field (a) perpendicular to the hexagonal c axis and (b) parallel to the c axis at $T = 1.3$ K in 3R-$AgFeO_2$. (c) and (d) are the data for 2H-$AgFeO_2$. The inset in (b) show the data measured with powder sample of 3R-$AgFeO_2$. Triangle symbols show the phase transition fields.

On the other hand, the multistep metamagnetic behavior was observed in B_c. The critical fields are B_c = 12.5 T($\equiv B_{c1}$), 27.0 T($\equiv B_{c2}$), 38.0 T($\equiv B_{c3}$) and 49.5 T ($\equiv B_{c4}$), The first, second, fourth field-induced phase transitions show hysteresis, indicating first order phase transitions, while the third one has no hysteresis, suggesting a second order transition. The magnetization values are $\sim 1\ \mu_B$ (1/5 of 5 μ_B of Fe^{3+}) for $B_{c1} \leq B_c \leq B_{c2}$, and $\sim 1.67\ \mu_B$ (1/3 of 5 μ_B) for $B_{c2} \leq B_c \leq B_{c3}$. Compared with the similar magnetization process of the well studied 3R-$CuFeO_2$ case, we can expect the collinear five-sublattice (5SL) ↑↑↑↓↓ and the three-sublattice (3SL) ↑↑↓

for $B_{c1} \leq B_c \leq B_{c2}$ and $B_{c2} \leq B_c \leq B_{c3}$, respectively. The details of the 5SL and 3SL structures are described in previous paper.[36,42] For $B_{c3} \leq B_c \leq B_{c4}$, we can expect a noncollinear canted-3SL from the linear increasing magnetization, while the conical structure was predicted for $B_c \geq B_{c4}$.[37] Magnetization process for the powder sample also exhibits these anomalies with broader peak shapes in dM/dB as shown in the inset of Fig. 4 (b). The detailed comparison in the magnetization process of 3R-$AgFeO_2$ with 3R-$CuFeO_2$ is discussed in the section IV.

2H-$AgFeO_2$– Figures 3(c) and 3(d) show the temperature dependences of magnetization in B_{ab} and B_c up to 6 T in 2H-$AgFeO_2$. A small peak and a steep drop anomalies were found at T = 17 K and T =9.4 K at $B_{ab} = B_c = 0.1$ T, respectively. As also seen in the case of 3R-$AgFeO_2$, the phase transition temperatures of the single crystal sample are slightly lower than those of the powder sample reported in previous paper (18 K and 11 K) in 2H-$AgFeO_2$.[28] It should be noted that the phase transitions observed in the magnetization data of the single crystal are much clearer than those of the previous powder data with the phase coexistence. The magnetic fields, B_{ab} and B_c up to 6 T , do not affect the phase transition temperatures significantly.

The magnetization processes of 2H-$AgFeO_2$ are completely different from those of 3R-$AgFeO_2$, which are shown in Figs. 4(c) and 4(d). It infers that exchange parameters are significantly different from those of 3R-$AgFeO_2$. In B_{ab}, the metamagnetic phase transition was observed around B_{ab} = 35 T, which has a large hysteresis. The data for B_c also exhibits a single phase transition with the large hysteresis around B_c = 20 T. Unlike 3R-$AgFeO_2$, magnetization plateaus are not seen in 2H-$AgFeO_2$. It suggests that noncollinear magnetic orderings are realized in the high magnetic field phases existing $B_{ab} \geq 35$ T and $B_c \geq 20$ T as well as the lower field phase.

B. Dielectric properties

3R-$AgFeO_2$– We measured the dielectric permittivity and the pyroelectric current associated with the magnetic phase transitions. In 3R-$AgFeO_2$, we observed step anomalies at T = 14 K and T = 5.5 K in the dielectric permittivity along both directions parallel and perpendicular to the *ab* plane, as shown in Figs. 5(a) and 5(b). We observed the ferroelectric polarizations below T = 5.5 K for both the directions, as shown in Fig. 5(c). Although the direction of polarization had been unknown in the previous powder work,[24] we found that the polarization contains the two components, P_{ab} and P_c in the present single crystal study. The polarization values are P_{ab} ~300 μC/m^2 and P_c ~100 μC/m^2, which do not reach the maximum values with the poling electric field up to 267 kV/m and 800 kV/m, respectively, as shown in the inset of Fig. 5(c). By application of magnetic field at 4.2 K, the ferroelectric polarization disappears at $B_c \simeq$ 13 T (Fig. 5(d)), which is associated with the phase transition from the ICM2 phase to collinear 5SL ↑↑↑↓↓ phase with nonpolar point group.

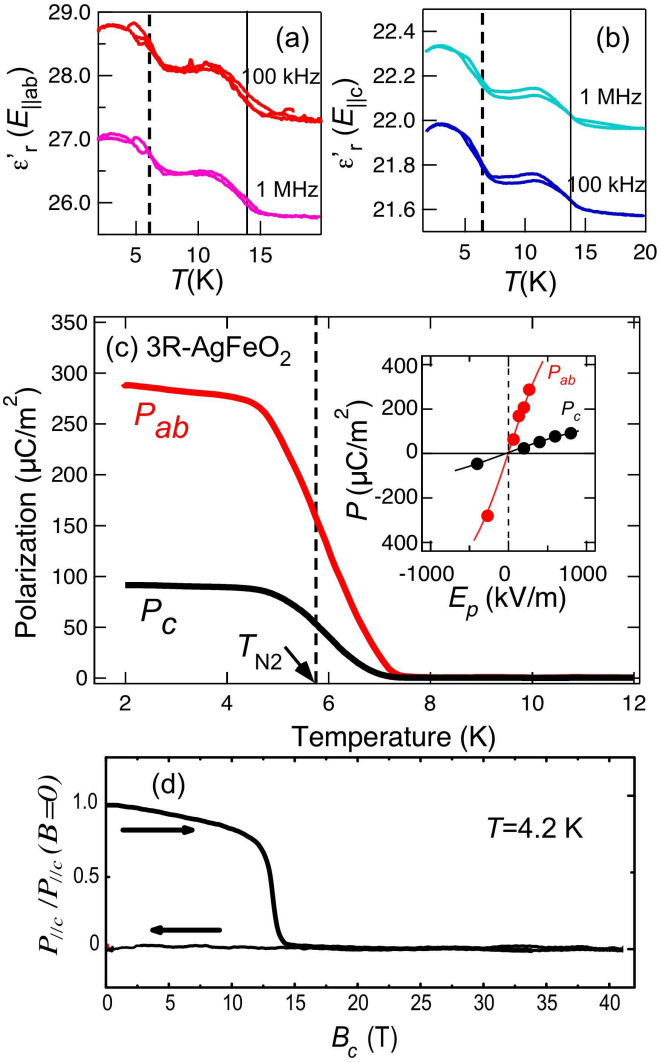

FIG. 5: (color online) Temperature dependence of dielectric permittivity (a) perpendicular to the hexagonal c axis and (b) parallel to the c axis in 3R-$AgFeO_2$. (c) Temperature dependence of electric polarization perpendicular to the hexagonal c axis and parallel to the c axis, which were measured after poling in electric field, 267 kV/m and 800 kV/m, respectively. The inset in (c) is poling electric field dependence of electric polarization along both the directions. (d) Magnetic field dependence of the electric polarization along the c axis at T = 4.2 K.

2H-$AgFeO_2$– In contrast, we did not observe any anomalies around the phase transition temperature in dielectric permittivity, suggesting that spin-lattice coupling is weak in 2H-$AgFeO_2$ compared with that in 3R-$AgFeO_2$. In the pyroelectric current measurements, we did not find any peak anomaly around the magnetic phase transition temperatures for 2H-$AgFeO_2$ within the

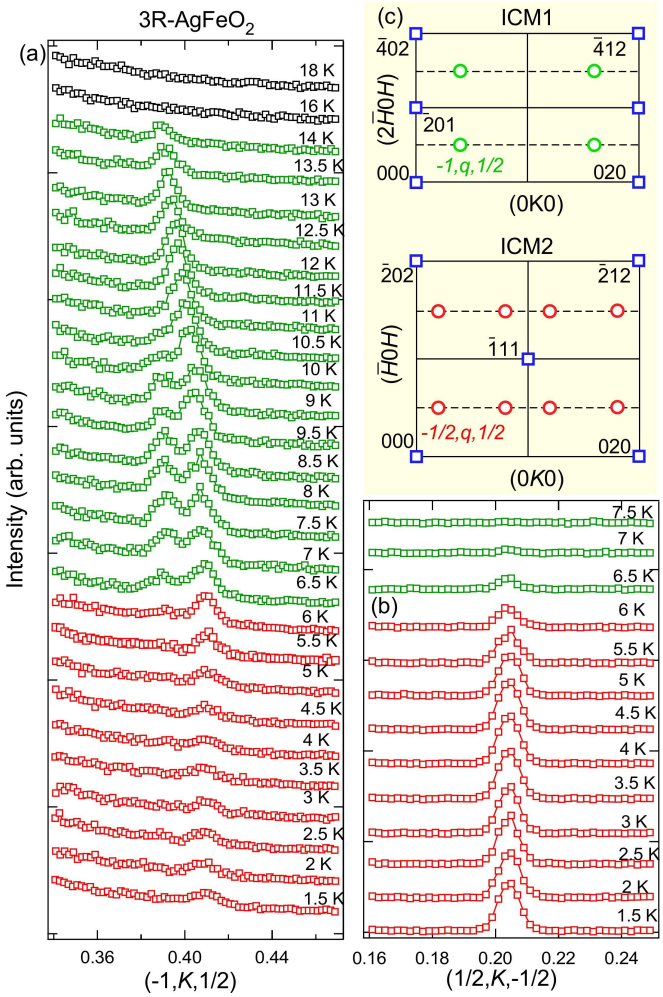

FIG. 6: (color online) Temperature dependence of neutron diffraction profile along the reciprocal lattice line (a) $[\bar{1}, K, \frac{1}{2}]$ and (b) $[\frac{1}{2}, q, \frac{\bar{1}}{2}]$ in 3R-$AgFeO_2$. (c) Schematic illustrations of the reciprocal lattice planes, $(2\bar{H}, K, H)$ for ICM1 phase, and $(\bar{H}, K, H)$ for ICM2 phase. Square and circle symbols denote nuclear and magnetic reflections points.

experimental accuracy.

C. Neutron diffraction

3R-AgFeO$_2$ – The temperature dependence of magnetic neutron diffraction profiles along the reciprocal lattice $[\bar{1}, K, \frac{1}{2}]$ line is shown in Fig. 6(a). The diffraction peak assigned as the incommensurate $(\bar{1}, q, \frac{1}{2})$ with $q \simeq 0.4$ appears below $T = 14$ K, which corresponds to the higher phase transition from the paramagnetic phase to ICM1 phase. The wave number q significantly depends on temperature from q =0.39 at $T = 14$ K and fixes to $q = 0.41$ below $T \sim 7$ K, as clearly seen in Fig. 7(b). The temperature dependent propagation vector in the ICM1 phase, $\boldsymbol{k} = (\bar{1}, q, \frac{1}{2})$, is consistent with that observed for the powder sample,[24] suggesting that the collinear SDW structure is realized in the single crystal sample. An additional reflection with very close to $q \simeq 0.39$ onsets below 10 K in the ICM1 phase, indicating that a magnetic ordering with the slightly different $\boldsymbol{k}$-vector appears. This is similarly seen as the peak broadening observed in the powder sample.[24] The coexistence behavior has been also found near first order phase transition for another frustrated system, which can be explained by the strong competition between frustrated exchange interaction and thermal fluctuations.[38]

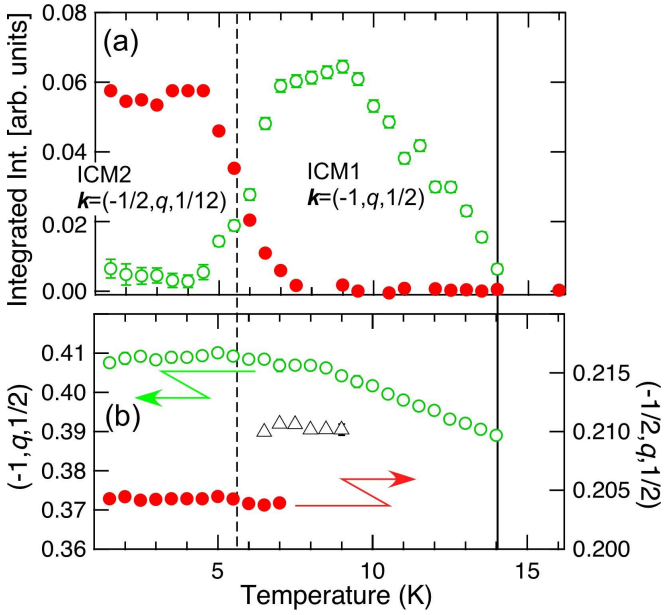

FIG. 7: (color online) (a)Temperature dependence of (a)integrated intensity of magnetic reflections indexed by $\boldsymbol{k} = (\bar{1}, q, \frac{1}{2})$ and $\boldsymbol{k} = (\frac{\bar{1}}{2}, q, \frac{1}{2})$ in 3R-$AgFeO_2$. (b)Temperature dependence of the incommensurate wave number (b component) in the $\boldsymbol{k}$-vector.

With further decreasing temperature, the intensity of reflections for ICM1 phase significantly decreases below T =6.0 K and the reflection persists at the lowest temperature T =1.5 K. At the same time, the diffraction peak at $(\frac{1}{2}, 0.205, -\frac{1}{2})$ is observed (Figs. 6(b) and 7(a)) below $T = 6.0$ K, which corresponds to the phase transition from ICM1 to ICM2 phases. The $\boldsymbol{k} = (-\frac{1}{2}, q, \frac{1}{2})$ is consistent with that in the ICM2 phase observed in the powder sample.[24] The magnetic Bragg peak positions are drawn on the reciprocal lattice planes shown in Fig. 6(c). The wave number q in ICM2 phase is independent of temperature as shown in Fig. 7(b). From the consistency in the $\boldsymbol{k}$-vector in ICM2 phase between single crystal and powder samples, it can be naturally considered that the cycloid magnetic ordering is realized in ICM2 phase in the single crystal sample. Magnetic structure analysis in 3R-$AgFeO_2$ could not be performed, due to lack of sufficient number observable magnetic reflections in the present experiment.

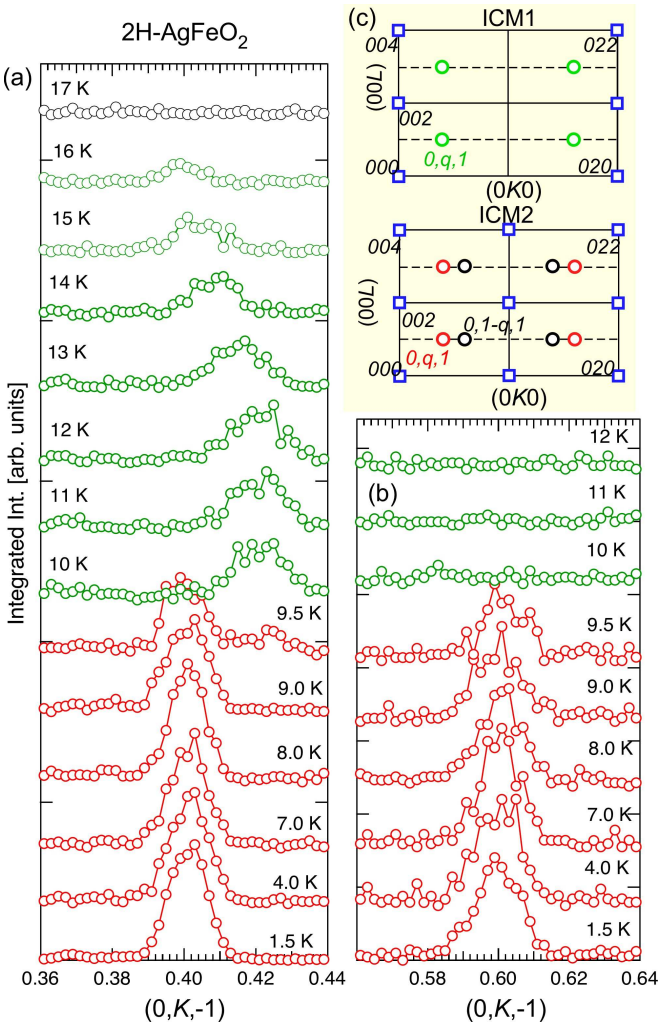

FIG. 8: (color online) Temperature dependence of neutron diffraction profile along the reciprocal lattice line (a) $[0, K, \bar{1}]$ and (b) $[0, q, \bar{1}]$ in 2H-$AgFeO_2$. (c) Schematic illustrations of the reciprocal lattice planes, $(0, K, L)$ for ICM1 and ICM2 phases. Squire and circle symbols denote nuclear and magnetic reflections points.

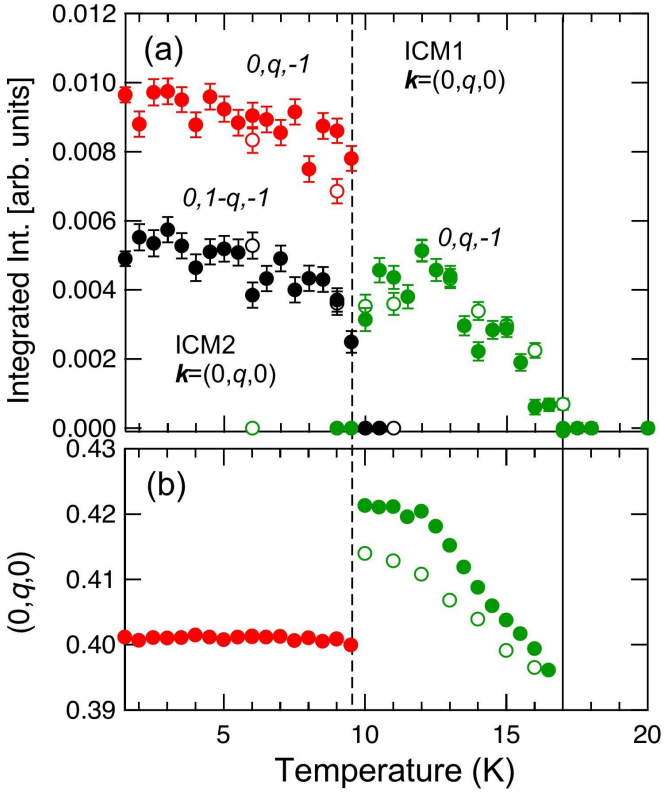

FIG. 9: (color online) (a)Temperature dependence of (a)integrated intensity of magnetic reflections indexed by $\boldsymbol{k} = (0, q, 0)$ in 2H-$AgFeO_2$. (b)Temperature dependence of the incommensurate wave number (b component) in the $\boldsymbol{k}$-vector. Closed and open symbols denote the data measured with warming and cooling processes, respectively.

2H-$AgFeO_2$– Temperature dependence of the neutron diffraction profile for 2H-$AgFeO_2$ is shown in Figs. 8(a) and 8(b). Below $T = 17$ K, a magnetic reflection starts to appear at $(0, 0.4, -1)$, corresponding to the magnetic phase transition from the paramagnetic phase to the ICM1 phase in 2H-$AgFeO_2$. The $\boldsymbol{k}$-vector can be determined to $\boldsymbol{k} = (0, q, 0)$ in the ICM1 phase, which is consistent with the SDW ordering of the powder sample.[28] We observe the strong temperature dependence in q in ICM1 phase, as shown in Figs. 8(a) and 9(b).

Below $T = 9.5$ K, a set of magnetic reflections are clearly found at (0,0.4,-1) and (0,0.6,-1) instead of varnishing the reflections of ICM1 phase, corresponding to the phase transition from ICM1 to the other phase named ICM2. (Figs. 8(b) and 7(b)) We can define the $\boldsymbol{k}$-vector to be $\boldsymbol{k} = (0, q, 0)$ with temperature independent $q = 0.4$ (Fig. 7(b)). In the previous powder experiment, two magnetic phases coexist at low temperature, which include the proper screw phase (ICM2) with $\boldsymbol{k} = (0, q, 0)$ with $q = 0.4$, and the general spiral phase (ICM3) with $\boldsymbol{k} = (q_a, q_b, q_c)$.[28] The $\boldsymbol{k}$-vector observed in the present study is in agreement with the proper screw phase in the powder study. The ICM3 phase seen in the powder sample was not observed in the present single crystal experiment, meaning that the single magnetic ground state of ICM2 phase is realized in the single crystal of 2H-$AgFeO_2$. The ICM3 phase might be induced by a small amount of impurity in the powder sample.[28]

In order to determine the magnetic structure in the ICM2 phase of 2H-$AgFeO_2$, we performed the magnetic structure analysis with using observed magnetic and nuclear reflections at T =1.5 K. We compared the experimental data, corrected by Lorentz factor, with magnetic structure factors calculated from noncollinear spin models. It should be noted that the reciprocal lattice points where the observed satellite reflections start are at not only the symmetry allowed $H + K = 2n$ (n =integer) but also the forbidden $H + K = 2n + 1$ in the $Ccmm$

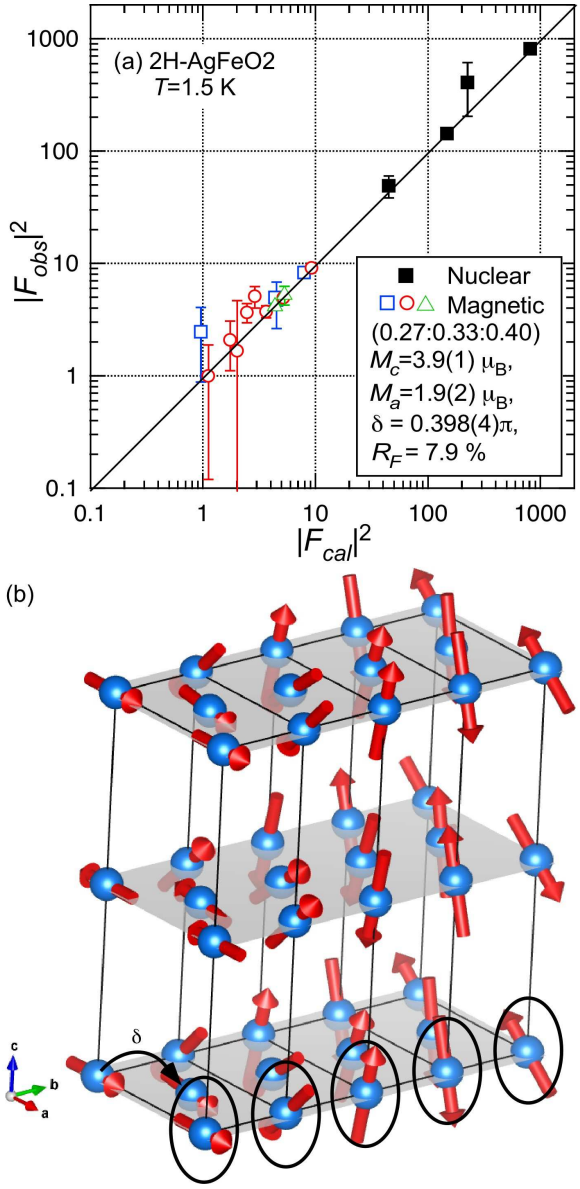

FIG. 10: (color online) (a)Result of the refinement for the data acquired at $T = 1.5$ K in 2H-$AgFeO_2$. The open and closed symbols denote magnetic and nuclear reflections, and the difference in the symbols for magnetic data corresponds to different domains. The refined magnetic structure parameters, magnetic domain population, magnetic moments (M_c and M_a), initial phase shift (δ), and reliability factor (R_F), are listed in the inset. (b)Illustrations of the determined magnetic structure, proper screw structure with ellipsoidal distortion for ICM2 phase in 2H-$AgFeO_2$.

space group for ICM2 phase. This observation implies a presence of structure distortion violating the C-centering condition and indicates a further symmetry reduction at least down to $Pmma$. The distortion can be expressed by $Y1+$ irreducible representation (IR) (in the ISODISTORT notations[39,40]). The symmetry lowering should make two Fe^{3+} sites, (0,0,0) and $(\frac{1}{2},\frac{1}{2},0)$ ((0,0,$\frac{1}{2}$) and $(\frac{1}{2},\frac{1}{2},\frac{1}{2})$) in the orthorhombic unit cell, inequivalent, leading to the independent initial phase in the incommensurate modulation at the two sites. The phase difference between them is defined to be δ. As shown in Figs. 10(a) and 10(b), the magnetic structure in the ICM2 phase of 2H-$AgFeO_2$ has been determined to the proper screw structure with ellipsoidal distortion with the reliability factor $R_F = 7.8$ %. The order parameter of the proper screw structure can be expressed by combination of time-odd IRs of the $Pmma$ space group, $mDT_3 \oplus mDT_4$ (in the ISODISTORT notations[39,40]). The refined parameters are the amplitudes of magnetic moments along the a-axis and c-axis, $M_a = 1.9\ \mu_B$ and $M_c = 3.2\ \mu_B$, and the initial phase shift $\delta = 0.39\pi$. The refined δ value corresponds to the ferromagnetic arrangement between (0,0,0) and $(\frac{1}{2},\frac{1}{2},0)$, and (0,0,$\frac{1}{2}$) and $(\frac{1}{2},\frac{1}{2},\frac{1}{2})$.(Fig. 10(b)) The determined magnetic structure is consistent with the result obtained in the powder study.[28] The symmetry of the ICM2 phase is also described by the $P2_1221'(0,0,\gamma)00ss$, $\gamma = q$ magnetic superspace group,[39,40] indicating that the magnetic order parameter breaks all the mirror plane symmetries but keeps the two fold rotational symmetries along the three orthogonal directions, resulting in the nonpolar magnetic point group $2221'$. This is consistent with the absence of the electric polarization below $T = 9.5$ K. The magnetic structure of the ICM2 phase determined in the present work for the 2H-$AgFeO_2$ polytype is similar to the magnetic polar phase found in 3R-$CuFe_{1-x}Ga_xO_2$.[4,13,41] However, the magnetic point gruops are different from each other, nonpolar $2221'$ in 2H-$AgFeO_2$ and polar $21'$ in 3R-$CuFe_{1-x}Ga_xO_2$. The difference relates to the hexagonal and rhombohedral parent symmetries, resulting in the absence and emergence of the ferroelectricity, respectively.

IV. DISCUSSION

A. exchange interactions and anisotropy

3R-$AgFeO_2$ exhibits multi-step magnetization changes by the application of magnetic field along the hexagonal c axis, which is very similar to that of the other delafossite ferrite 3R-$CuFeO_2$ apart from quantitative difference in critical fields.[37,42–44] Therefore, we can thus infer that 3R-$AgFeO_2$ is considered to be a triangular lattice antiferromagnet with exchange interactions up to third-nearest neighbors[45] with slightly modified exchange and anisotropic parameters from those in 3R-$CuFeO_2$. The critical magnetic fields for 3R-$AgFeO_2$ and 3R-$CuFeO_2$ are summarized in Table 1. From the magnetization process in 3R-$AgFeO_2$, we can expect the critical magnetic field where the magnetization reaches 5 μ_B of Fe^{3+} to be $\sim$ 85 T (defined as B_{c5}) by extrapolating the magnetization slope above $B_c = 50$ T. Therefore, the total anitferromagnetic exchange interaction in 3R-$AgFeO_2$ is larger than 3R-$CuFeO_2$ with $B_{c5} = 75$ T, which is consis-

tent with the larger Weiss temperature value of Θ =-140 K in 3R-$AgFeO_2$ compared with -90 K in 3R-$CuFeO_2$. This tendency is also seen in the critical fields, B_{c2} and B_{c3}, as shown in Table I.

In contrast, we found some differences in the critical fields for B_{c0}, B_{c1} and B_{c4}, which cannot be explained by the overall shift of exchange energy between the two compounds. Firstly, a spin flop phase transition seen at B_{c0} = 7 T in 3R-$CuFeO_2$ was not observed in 3R-$AgFeO_2$. Reflecting the collinear, ↑↑↓↓, magnetic ground state in zero field, 3R-$CuFeO_2$ shows zero magnetization plateau up to B_c = 7 T followed by a spin flop phase transition to the noncollinear proper screw phase with a finite gradient of magnetization. For 3R-$AgFeO_2$, the noncollinear cycloid ordering in zero field gives linear increasing of magnetization. The spin flop transition is caused by competition between the easy axis anisotropy and Zeeman energy, suggesting the anisotropy in 3R-$AgFeO_2$ is smaller than that in 3R-$CuFeO_2$, leading to the disappearance of the collinear ground state in zero field and spin flop transition in 3R-$AgFeO_2$.

Secondly, B_{c1} and B_{c4} in 3R-$AgFeO_2$ are smaller than those of 3R-$CuFeO_2$ in spite of larger overall antiferromagnetic exchange interaction in 3R-$AgFeO_2$. At B_{c1}, a magnetic phase transition occurs from noncollinear, cycloid in 3R-$AgFeO_2$ and proper screw in 3R-$CuFeO_2$, to collinear 5SL (↑↑↑↓↓) phase. At B_{c4}, a phase transition occurs from noncollinear canted-3SL to conical spin state as shown in Ref.[37] at B_{c4}. Since both phase transitions at B_{c1} and B_{c4} are associated with either noncollinear to collinear, or one noncollinear to another noncollinear spin states, we can infer that the anisotropy energy is also an important factor for the critical field values. In 3R-$CuFe_{1-x}X_xO_2$ (X =Al or Ga) with the chemical doping, the similar behaviors are seen, like the disappearance of the spin-flop phase transition at B_0, and the critical fields reduction for B_{c1} and B_{c4}. In 3R-$CuFe_{0.085}Al_{0.015}O_2$, the critical fields are the smaller values B_{c1} = 11.5 T and B_{c4} = 48 T.[48] Actually, in inelastic neutron scattering studies, the single ion anisotropy constant D is reduced from 0.064 meV in 3R-$CuFeO_2$ to 0.007 meV in 3R-$CuFe_{0.985}Ga_{0.035}O_2$.[49,50] Therefore, we can expect that the anisotropy energy in 3R-$AgFeO_2$ is also weaker than that in 3R-$CuFeO_2$. For further understanding the exchange interactions and anisotropy, inelastic neutron scattering and electron spin resonance studies for 3R-$AgFeO_2$ are needed.

For 2H-$AgFeO_2$, in spite of almost the same exchange networks in the triangular lattice plane as 3R-$AgFeO_2$, the magnetization processes are completely different from each other. The nearest neighbor exchange interaction, $J1$, is known as sum of Fe-O-Fe $\sim 90°$ antiferromagnetic superexchange and Fe-Fe direct ferromagnetic exchange interactions in delafossite system.[33] Considering the Fe-O-Fe bond angle and Fe-Fe distance are nearly the same values, 96.54° and 3.039 Å in 2H-$AgFeO_2$,[28] and 96.5° and 3.033 Å in 3R-$AgFeO_2$,[24,51] we can expect the almost the same $J1$ value. However, for the next nearest neighbor, $J2$, the third nearest neighbor interactions, $J3$, in the triangular lattice plane, and the inter-layer exchange interactions, these exchange paths are unknown and expected to be much more complex than the case of $J1$. Therefore, the difference in stacking sequence of the triangular lattice layers along the hexagonal c axis between 2H-$AgFeO_2$ and 3R-$AgFeO_2$ is considered to significantly affect those exchange interactions, leading to the completely different magnetization process in 2H-$AgFeO_2$.

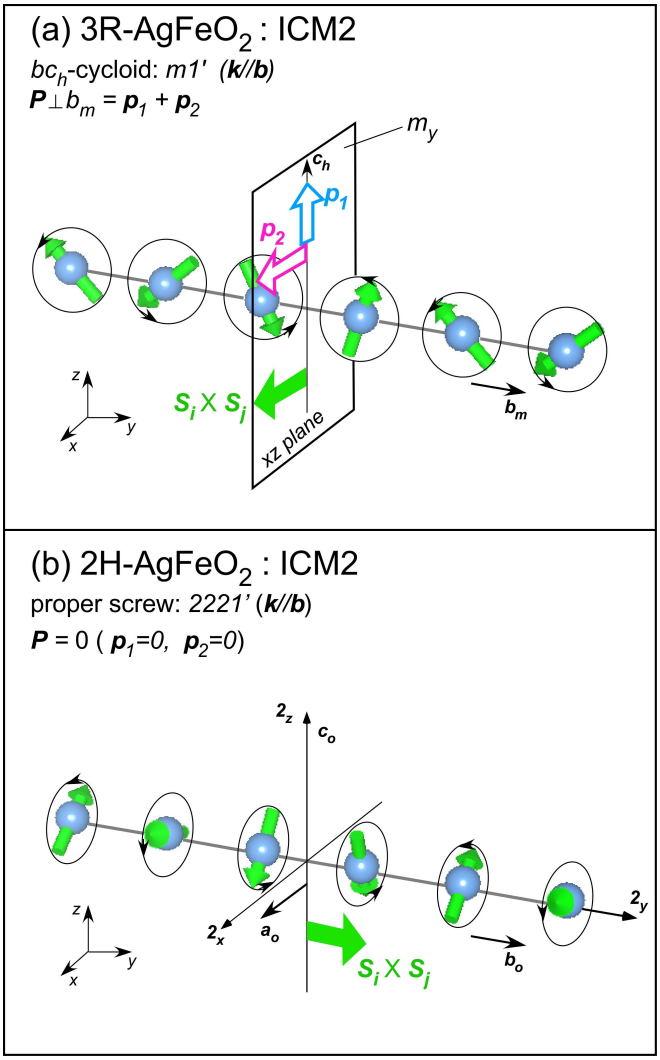

FIG. 11: (color online) Schematic illustrations representing the relationships between noncollinear spin modulation along the b-axis and the electric polarization directions determined by the extended inverse-DM mechanism,[19] $\boldsymbol{p}_1 \propto \boldsymbol{r}_{ij} \times [\boldsymbol{S}_i \times \boldsymbol{S}_j]$ and $\boldsymbol{p}_2 \propto \boldsymbol{S}_i \times \boldsymbol{S}_j$ for (a) the cycloid phase in 3R-$AgFeO_2$ and (b) the proper screw phase in 2H-$AgFeO_2$.

TABLE I: (color online) List of critical magnetic fields and Weiss temperature for 3R-$CuFeO_2$ and 3R-$AgFeO_2$. (*)The critical field B_{c5} was predicted by extrapolating the experimental data above B_c =50 T in 3R-$AgFeO_2$.

	B_{c0}(T)	B_{c1}(T)	B_{c2}(T)	B_{c3}(T)	B_{c4}(T)	B_{c5}(T)	Θ(K)	Reference
3R-$CuFeO_2$	7	13	20	34	54	75	-90[46]	Refs.[37,42–44]
3R-$AgFeO_2$	–	12.5	27	38	49.5	85*	-140[47]	This work

B. ferroelectric polarization

Let us discuss the direction of ferroelectric polarization in 3R-$AgFeO_2$ and absence of a polarization in 2H-$AgFeO_2$. In the present experiments, the ferroelectric polarization with two components P_{ab} and P_c were observed in ICM2 phase of 3R-$AgFeO_2$, which is concomitant with the onset of the cycloid magnetic ordering with spins in the bc_h-plane (c_h is the hexagonal c axis) and $m1'$ magnet point group. In contrast, the electric polarization was not observed in the proper screw phase (ICM2), with spins in the ac-plane and $2221'$, in 2H-$AgFeO_2$. As mentioned in the introduction, in the well known spin current[7] and inverse DM[5,6] theories, the polarization is expressed by $\boldsymbol{p}_1 \propto \boldsymbol{r}_{ij} \times (\boldsymbol{S}_i \times \boldsymbol{S}_j)$, and is expected to be perpendicular to both $\boldsymbol{r}_{ij}$ and $\boldsymbol{S}_i \times \boldsymbol{S}_j$. When a crystal has neither a mirror plane containing $\boldsymbol{r}_{ij}$ nor an n-fold rotation axis perpendicular to $\boldsymbol{r}_{ij}$, the electric polarization can be expected to be parallel to the cross-product, $\boldsymbol{p} \propto \boldsymbol{S}_i \times \boldsymbol{S}_j (\equiv \boldsymbol{p}_2)$, via the inverse DM effect, as proposed by Kaplan and Mahanti.[19] This symmetry condition can be also explained by that a crystal belongs to ferroaxial point group.[22] In the case of 3R-$AgFeO_2$ with $R\bar{3}m$, the magnetic propagation vector such as $(q, q, 0)$ in the hexagonal basis, breaks the three-fold rotational symmetry and lowers the symmetry to the monoclinic $C2/m$. It is convenient to use the extended $\boldsymbol{k}$-vector group to discuss the symmetry-allowed components of the spin-induced polarization.[4,24] The $C2/m$ space group with the ferroaxial point group, $2/m$, does not possess a mirror plane containing $\boldsymbol{r}_{ij}$ and an n-fold rotation axis perpendicular to $\boldsymbol{r}_{ij}$, leading to making the $\boldsymbol{p}_2$ component allowed. Actually, the observations of P_c and P_{ab} in ICM2 phase of 3R-$AgFeO_2$ are in agreement with $\boldsymbol{p}_1$ and $\boldsymbol{p}_2$ components, respectively, as illustrated in Fig. 11(a). In contrast, in 2H-$AgFeO_2$, the parent space group is $P6_3/mmc$ and the extended wave vector group of the $(q, q, 0)$ is orthorhombic $Ccmm$ (non-ferroaxial), which has a mirror planes containing $\boldsymbol{r}_{ij}$ and two-fold rotation axes perpendicular to $\boldsymbol{r}_{ij}$. In this case, the second term $\boldsymbol{p}_2$ is not allowed. Taking account of that the proper screw ordering has $\boldsymbol{S}_i \times \boldsymbol{S}_j$ parallel to $\boldsymbol{r}_{ij}$, the $\boldsymbol{p}_1$ term is also zero, we can expect the absence of ferroelectricity in the ICM2 phase of 2H-$AgFeO_2$, as the polarization was not observed in the present experiment. (Fig. 11(b))

V. CONCLUSION

In conclusion, we have investigated magnetic and dielectric properties of rhombohedral 3R-$AgFeO_2$ and hexagonal 2H-$AgFeO_2$, by using magnetic and dielectric bulk measurements and neutron diffraction experiment with single crystals grown by the hydrothermal synthesis. Although the two dimensional triangular lattice layers of Fe^{3+} are common in the two polytypes, the magnetic and ferroelectric properties are significantly different. The magnetization process in 3R-$AgFeO_2$ exhibits 1/5 and 1/3 magnetization plateaus similar to 3R-$CuFeO_2$, while that of 2H-$AgFeO_2$ is completely different. Therefore, 3R-$AgFeO_2$ is considered to be a triangular lattice antiferromagnet with exchange interactions up to third-nearest neighbors with slightly modified exchange and anisotropic parameters from those in 3R-$CuFeO_2$. On the other hand, in 2H-$AgFeO_2$, the exchange interactions are significantly modified by the difference in the stacking sequence of triangular lattice plane. Moreover, the ferroelectric polarization components, parallel and perpendicular to the hexagonal c axis, were observed in the cycloid phase in 3R-$AgFeO_2$, as predicted in the generalized inverse-DM mechanism including $\boldsymbol{p}_1 \propto \boldsymbol{r}_{ij} \times (\boldsymbol{S}_i \times \boldsymbol{S}_j)$ and $\boldsymbol{p}_2 \propto \boldsymbol{S}_i \times \boldsymbol{S}_j$. Unlike 3R-$CuFeO_2$, the ferroelectric polarization is absent in the proper screw phase in 2H-$AgFeO_2$, since the $\boldsymbol{p}_2$ term is not allowed in the case of the hexagonal parent space group.

Acknowledgements

The images shown in Figs. 1, 10 and 11 were depicted using the VESTA[52] software program developed by K. Momma. This work was supported by a JSPS KAKENHI grants (No. 15H05433, and 16K05413) as well as the TUMOCS project, which has received funding from the European Union Horizon 2020 Research and Innovation Program under the Marie Sklodowska-Curie grant agreement (no. 645660).

* Electronic address: TERADA.Noriki@nims.go.jp
† Electronic address: hirohiko@phys.chuo-u.ac.jp

[1] T. Kimura, T. Goto, H. Shintani, K. Ishizaka, T. Arima and Y. Tokura, Nature **426**, 55 (2003).

[2] S.-W Cheong and M. Mostovoy, Nature Mater. **6**, 13 (2007).
[3] Y. Tokura and S. Seki, Adv. Mater. **22**, 1554 (2010).
[4] N. Terada, J. Phys.: Cond. Mat. **26**, 453202 (2014).
[5] M. Mostovoy, Phys. Rev. Lett. **96**, 067601 (2006).
[6] I.A. Sergienko and E. Dagotto, Phys. Rev. B **73**, 094434 (2006).
[7] H. Katsura, N. Nagaosa and A. V. Balatsky, Phys. Rev. Lett. **95**, 057205 (2005).
[8] M. Kenzelmann, A. B. Harris, S. Jonas, C. Broholm, J. Schefer, S. B. Kim, C. L. Zhang, S-W. Cheong, O. P. Vajk, and J. W. Lynn, Phys. Rev. Lett. **95**, 087206 (2005).
[9] T. Arima, A. Tokunaga, T. Goto, H. Kimura, Y. Noda and Y. Tokura, Phys. Rev. Lett. **96**, 097202 (2006).
[10] T. Kimura, J. C. Lashley and A. P. Ramirez, Phys. Rev. B **73**, 220401(R) (2006).
[11] S. Kanetsuki, S. Mitsuda, T. Nakajima, D. Anazawa, H. A. Katori, and K. Prokes, J. Phys. Condens. Matter **19**, 145244 (2007).
[12] S. Seki, Y. Yamasaki, Y. Shiomi, S. Iguchi, Y. Onose and Y. Tokura, Phys. Rev. B **75**, 100403(R) (2007).
[13] N. Terada, T. Nakajima, S. Mitsuda, H. Kitazawa, K. Kaneko and N. Metoki, Phys. Rev. B **78**, 014101 (2008).
[14] T. Nakajima, S. Mitsuda, S. Kanetsuki, K. Tanaka, K. Fujii, N. Terada, M. Soda, M. Matsuura, and K. Hirota, Phys. Rev. B **77**, 052401 (2008).
[15] T. Nakajima, S. Mitsuda, K. Takahashi, M. Yamano, K. Masuda, H. Yamazaki K. Prokes, K. Kiefer, S. Gerischer, N. Terada H. Kitazawa, M. Matauda, K. Kakurai, H. Kimura, Y. Noda, M. Soda, M. Matsuura, and K. Hirota Phys. Rev. B **79**, 214423 (2009).
[16] S. Seki, Y. Onose and Y. Tokura, Phys. Rev. Lett. **101**, 067204 (2008).
[17] K. Kimura, H. Nakamura, K. Ohgushi and T. Kimura, Phys. Rev. B **78**, 140401(R) (2008).
[18] M. Soda, K. Kimura, T. Kimura, M. Matsuura and K. Hirota, J. Phys. Soc. Jpn. **78**, 124703 (2009).
[19] T. A. Kaplan and S. D. Mahanti, Phys. Rev. B **83**, 174432 (2011).
[20] M. Kenzelmann, G. Lawes, A. B. Harris, G. Gasparovic, C. Broholm, A. P. Ramirez, G. A. Jorge, M. Jaime, S. Park, Q. Huang, A. Ya. Shapiro, and L. A. Demianets, Phys. Rev. Lett. **98**, 267205 (2007).
[21] A. J. Hearmon, F. Fabrizi, L. C. Chapon, R. D. Johnson, D. Prabhakaran, S. V. Streltsov, P. J. Brown and P. G. Radaelli, Phys. Rev. Lett. **108**, 237201 (2012).
[22] R. D. Johnson, Sunil Nair, L. C. Chapon, A. Bombardi, C. Vecchini, D. Prabhakaran, A. T. Boothroyd and P. G. Radaelli, Phys. Rev. Lett. **107**, 137205 (2011).
[23] M. Tokunaga, M. Akaki, T. Ito, S. Miyahara, A. Miyake, H. Kuwahara, and N. Furukawa, Nat. Comm. **6**, 5878 (2016).
[24] N. Terada, D. D. Khalyavin, P. Manuel, Y. Tsujimoto, K. Knight, P. G. Radaelli, H. S. Suzuki, and H. Kitazawa, Phys. Rev. Lett. **109**, 097203 (2012).
[25] N. Terada, D. D. Khalyavin, P. Manuel, Y. Tsujimoto, K. Knight, P. G. Radaelli, H. S. Suzuki, and H. Kitazawa, EPJ Web of Conferences **40**, 15008 (2013).
[26] R. Seshadri, C. Felser, K. Thieme, and W. Tremel, Chem. Mater. **10**, 2189 (1998).
[27] W. C. Sheets, E. Mugnier, A. Barnabé, Y. J. Marks, and K. R. Poeppelmeier, Chem. Mater. **18**, 7 (2006).
[28] N. Terada, D. D. Khalyavin, P. Manuel, Y. Tsujimoto, A. A. Belik, Phys. Rev. B. **91**, 094434 (2015).
[29] The Crystallographic Information Files for 3R-$AgFeO_2$ (113 K) and 2H-$AgFeO_2$ (293 K) obtained by the single crystal X-ray diffraction measurements are attached as supplementary information.
[30] D. Pandey and P. Krishna, *Polytypism in Close-Packed Structures, in Current Topics in Materials Science*, (E. Kaldis, ed.), pp. 415-491, North Holland Pub. Co., Amsterdam (1982).
[31] L. C. Chapon, P. Manuel, P. G. Radaelli, C. Benson, L. Perrott, S. Ansell, N. J. Rhodes, D. Raspino, D. Duxbury, E. Spill and J. Norris, Neutron News **22**, 22 (2011).
[32] J. Rodriguez-Carvajal, Physica B, **192**, 55 (1993).
[33] M. Mekata, N. Yaguchi, T. Takagi, T. Sugino, S. Mitsuda, H. Yoshizawa, N. Hosoito, and T. Shinjo, J. Phys. Soc. Jpn. **62**, 4474 (1993).
[34] S. Mitsuda, H. Yoshizawa, N. Yamaguchi, and M. Mekata, J. Phys. Soc. Jpn. **60**, 1885 (1991)
[35] S. Mitsuda, N. Kasahara, T. Uno and M. Mase, J. Phys. Soc. Jpn. **67**, 4026 (1998).
[36] S. Mitsuda, M. Mase, K. Prokes, H. Kitazawa and H. A. Katori, JPSJ, **69**, 3513 (2000)
[37] T. T. A. Lummen, C. Strohm, H. Rakoto, and P. H. M. van Loosdrecht, Phys. Rev. B **81**, 224420 (2010).
[38] N. Terada, S. Mitsuda, T. Fujii, K. Soejima, I. Doi, H. A. Katori and Y. Noda, J. Phys. Soc. Jpn. **74**, 2604 (2005).
[39] B. J. Campbell, H. T. Stokes, D. E. Tanner, and D. M. Hatch, J. Appl. Crystallogr. **39**, 607 (2006).
[40] J M Perez-Mato, J L Ribeiro, V Petricek and M I Aroyo, J. Phys.: Condens. Matter **24**, 163201 (2012).
[41] T. Nakajima, S. Mitsuda, K. Takahashi, M. Yamano, K. Masuda, H. Yamazaki, K. Prokes, K. Kiefer, S. Gerischer, N. Terada, H. Kitazawa, M. Matauda, K. Kakurai, H. Kimura, Y. Noda, M. Soda, M. Matsuura, and K. Hirota, Phys. Rev. B **79**, 214423 (2009).
[42] N. Terada, Y. Narumi, Y. Sawai, K. Katsumata, U. Staub, Y. Tanaka, A. Kikkawa, T. Fukui, K. Kindo, T. Yamamoto, R. Kanmuri, M. Hagiwara, H. Toyokawa, T. Ishikawa, and H. Kitamura, Phys. Rev. B **75**, 224411 (2007).
[43] S. Kimura, T. Fujita, N. Nishihagi, H. Yamaguchi, T. Kashiwagi, M. Hagiwara, N. Terada, Y. Sawai, and K. Kindo, Phys. Rev. B **84**, 104449 (2011).
[44] Z. Hua-Kun, S. Li-Ran, X. Zheng-Cai , H. Jun-Wei, C. Bo-Rong, J. Zhao, W. Meng, O. Zhong-Wen and C. Gang, Chin. Phys. Lett. **32**, 047502 (2015).
[45] R. S. Fishman, Phys. Rev. Lett. **106**, 037206 (2011).
[46] J. P. Doumerc, A. Wichainchai, A. Ammar, M. Pouchard and P. Hagenmuller, Mater. Res. Bull. **21**, 745 (1986).
[47] A. Vasiliev, O. Volkova, I. Presniakov, A. Baranov, G. Demazeau, J-M. Broto, M. Millot, N. Leps. R. Klingeler, B. Büchner, M. B. Stone and A. Zheludev, J. Phys. Condens. Matter **22**, 016007 (2009).
[48] T. Nakajima, S. Mitsuda, S. Kanetsuki, M. Yamano, S. Iwamoto, Y. Yoshida, H. Mitamura, Y. Sawai, M. Tokunaga, K. Kindo, K. Prokes, and A. Podlesnyak, Phys. Rev. B **81**, 014422 (2010).
[49] T. Nakajima, A. Sunou, S. Mitsuda, N. Terada, S. Kimura, K. Kaneko and H. Yamauchi, Phys. Rev. B **84**, 184401 (2011).
[50] T. Nakajima, S. Mitsuda, J. T. Haraldsen, R. S. Fishman, T. Hong, N. Terada, and Y. Uwatoko, Phys. Rev. B **85**, 144405 (2012).
[51] N. Terada, D. D. Khalyavin, P. Manuel, Y. Tsujimoto, K. Knight, P. G. Radaelli, H. S. Suzuki, and H. Kitazawa,

EPJ Web of Conferences **40**, 15008 (2013).
[52] K. Momma and F. Izumi, J. Appl. Crystallogr. **41**, 653 (2008).